UNIVERSITÄT PADERBORN
Die Universität der Informationsgesellschaft

Fakultät für Elektrotechnik, Informatik und Mathematik
Arbeitsgruppe Quanteninformatik

Classical Simulation of Quantum Circuits with Restricted Boltzmann Machines

Master's Thesis

in Partial Fulfillment of the Requirements for the Degree of

Master of Science

by

Jannes Stubbemann

submitted to:

Jun. Prof. Dr. Sevag Gharibian

and

Dr. Robert Schade

Paderborn, August 1, 2020

Declaration

(Translation from German)

I hereby declare that I prepared this thesis entirely on my own and have not used outside sources without declaration in the text. Any concepts or quotations applicable to these sources are clearly attributed to them. This thesis has not been submitted in the same or substantially similar version, not even in part, to any other authority for grading and has not been published elsewhere.

Original Declaration Text in German:

Erklärung

Ich versichere, dass ich die Arbeit ohne fremde Hilfe und ohne Benutzung anderer als der angegebenen Quellen angefertigt habe und dass die Arbeit in gleicher oder ähnlicher Form noch keiner anderen Prüfungsbehörde vorgelegen hat und von dieser als Teil einer Prüfungsleistung angenommen worden ist. Alle Ausführungen, die wörtlich oder sinngemäß übernommen worden sind, sind als solche gekennzeichnet.

City, Date

Signature

Contents

List of Figures

List of Algorithms

1 Notations

- sets with capital letters as X, V, H
- vectors have an arrow as $\vec{v}$
- i might either be an index or the imaginary number from the context

2 Quantum Computing

This chapter gives an introduction to the field of *Quantum Computation*. It covers the basics of qubits, quantum gates and circuits, and a high-level overview of quantum complexity classes. This chapter is based on [**?**], recommended as a reference for a more profound introduction into the field.

2.1 Qubits

While classical computers harness classical physical phenomena like electrical current to perform calculations, quantum computers harness *quantum mechanical* effects. The simplest quantum mechanical system is a quantum bit, or *qubit* for short. It is the fundamental building block of a quantum computer.

Mathematically, a qubit is a two-dimensional complex-valued unit vector, also called the *state vector* or *wave function* of the qubit:

$$|\psi\rangle = \begin{pmatrix} \alpha \\ \beta \end{pmatrix} \tag{2.1}$$

with *amplitudes* $\alpha, \beta \in \mathbb{C}$ and $\alpha^2 + \beta^2 = 1$. Rewriting $|\psi\rangle$ as

$$|\psi\rangle = e^{i\gamma} \left(\cos\frac{\theta}{2} |0\rangle + e^{i\rho} \sin\frac{\theta}{2} |1\rangle \right) \tag{2.2}$$

with $\theta, \rho, \gamma \in \mathbb{R}$ allows an intuitive interpration of a qubit as a point on the surface of the three-dimensional unit sphere, called the *Bloch Sphere*, which is visualized in figure **??**. The factor $e^{i\gamma}$ in front is called a *global phase* and can be ignored:

$$|\psi\rangle = \cos\frac{\theta}{2} |0\rangle + e^{i\rho} \sin\frac{\theta}{2} |1\rangle . \tag{2.3}$$

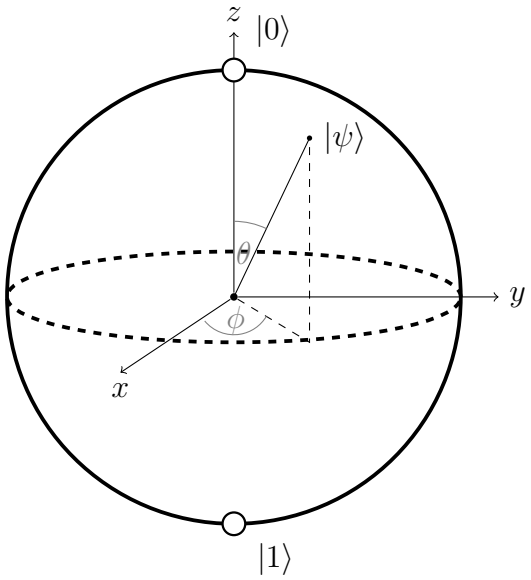

Figure 2.1: Bloch Sphere representation of a qubit state $|\psi\rangle$. $|\psi\rangle$ points to an arbitrary direction on the three dimensional unit sphere.

The states on the north and south pole of the Bloch Sphere are called the *computational basis states* defined as:

$$|0\rangle = \begin{pmatrix} 1 \\ 0 \end{pmatrix} \tag{2.4}$$

and

$$|1\rangle = \begin{pmatrix} 0 \\ 1 \end{pmatrix}. \tag{2.5}$$

These states correspond to the classical states 0 and 1 of a classical bit. Thus, another way of writing the wave function of a qubit, which is also the most practical one for quantum computation, is as a linear combination of the two computational basis states:

$$|\psi\rangle = \alpha \cdot |0\rangle + \beta \cdot |1\rangle. \tag{2.6}$$

A qubit whose amplitudes α and β are both non-zero is in a so-called *superposition* of the two computational basis states. A qubit in a superposition can be interpreted as being in both states $|0\rangle$ and $|1\rangle$ at the same time. This property is one of the underlying reasons why the classical simulation of quantum systems is computationally so hard and one of the sources of the potential computational power of quantum computers. It is not possible to read the values of the amplitudes α and β directly, however.

The qubit can only be in a superposition as long as it is completely isolated from its environment. Such a state is called a *coherent* state. As soon as the qubit

interacts with its environment, as it is necessary to read its value, it collapses randomly into one of the two computational basis states. All the information stored in the amplitudes before gets lost in this process.

In a quantum computer, the qubits are in a coherent state and potentially in a superposition during the computation. At the end of the computation, a so-called *projective measurement* is performed to read the states of the individual qubits. A projective measurement is given by *operators* $\mathbf{M} = M_i$, in our case $M_0 = |0\rangle\langle 0|$ and $M_1 = |1\rangle\langle 1|$. The probabilities $p(0)$ and $p(1)$ of observing a qubit in the $|0\rangle$ or $|1\rangle$ state are then defined by the amplitudes

$$\begin{aligned} p(0) &= \langle\psi| M_0^\dagger M_0 |\psi\rangle && (2.7)\\ &= \langle\psi| M_0 |\psi\rangle && (2.8)\\ &= \alpha \langle 0 \,|\, 0\rangle \langle 0| \alpha |0\rangle + \beta \langle 1 \,|\, 0\rangle \langle 0| \beta |1\rangle && (2.9)\\ &= \alpha^2 \langle 0 \,|\, 0\rangle \langle 0 \,|\, 0\rangle + \beta^2 \langle 1 \,|\, 0\rangle \langle 0 \,|\, 1\rangle && (2.10)\\ &= \alpha^2 && (2.11) \end{aligned}$$

and

$$\begin{aligned} p(1) &= \langle\psi| M_1^\dagger M_1 |\psi\rangle && (2.12)\\ &= \langle\psi| M_1 |\psi\rangle && (2.13)\\ &= \alpha \langle 0 \,|\, 1\rangle \langle 1| \alpha |0\rangle + \beta \langle 1 \,|\, 1\rangle \langle 1| \beta |1\rangle && (2.14)\\ &= \alpha^2 \langle 0 \,|\, 1\rangle \langle 1 \,|\, 0\rangle + \beta^2 \langle 1 \,|\, 1\rangle \langle 1 \,|\, 1\rangle && (2.15)\\ &= \beta^2 && (2.16) \end{aligned}$$

as $M_i^\dagger M_i = M_i$ and $\langle i \,|\, j\rangle = \delta_{ij}$.

After the measurement, the state of the qubit will be either

$$\left|\psi^\dagger\right\rangle = \frac{M_0 |\psi\rangle}{\sqrt{p(0)}} \tag{2.17}$$

or

$$\left|\psi^\dagger\right\rangle = \frac{M_1 |\psi\rangle}{\sqrt{p(1)}} \tag{2.18}$$

respectively, implying that the state of the qubit collapsed into one of the two computational basis states. Thus, any succinct measurement will result in the same outcome. In order to perform multiple measurements on the same state, it has to be prepared multiple times.

Two special qubit states which often occur in the domain of quantum computation are the $|-\rangle$ and $|+\rangle$ state defined as

$$|-\rangle = \frac{1}{\sqrt{2}} \cdot |0\rangle - \frac{1}{\sqrt{2}} \cdot |1\rangle \tag{2.19}$$

and

$$|+\rangle = \frac{1}{\sqrt{2}} \cdot |0\rangle + \frac{1}{\sqrt{2}} \cdot |1\rangle \,. \tag{2.20}$$

Those states differ in a *relative phase* and both have the same measurement statistics, lying between the states $|0\rangle$ and $|1\rangle$ on the Bloch Sphere:

$$\begin{aligned} p(0) &= \langle +| \, M_0 \, |+\rangle && (2.21)\\ &= \frac{1}{\sqrt{2}} \langle 0 \,|\, 0\rangle \, \langle 0| \, \frac{1}{\sqrt{2}} \, |0\rangle + \frac{1}{\sqrt{2}} \langle 1 \,|\, 0\rangle \, \langle 0| \, \frac{1}{\sqrt{2}} \, |1\rangle && (2.22)\\ &= \frac{1}{2} \langle 0 \,|\, 0\rangle \, \langle 0 \,|\, 0\rangle + \frac{1}{2} \langle 1 \,|\, 0\rangle \, \langle 0 \,|\, 1\rangle && (2.23)\\ &= \frac{1}{2} && (2.24) \end{aligned}$$

and

$$\begin{aligned} p(1) &= \langle +| \, M_1 \, |+\rangle && (2.25)\\ &= \frac{1}{\sqrt{2}} \langle 0 \,|\, 1\rangle \, \langle 1| \, \frac{1}{\sqrt{2}} \, |0\rangle + \frac{1}{\sqrt{2}} \langle 1 \,|\, 1\rangle \, \langle 1| \, \frac{1}{\sqrt{2}} \, |1\rangle && (2.26)\\ &= \frac{1}{2} \langle 0 \,|\, 1\rangle \, \langle 1 \,|\, 0\rangle + \frac{1}{2} \langle 1 \,|\, 1\rangle \, \langle 1 \,|\, 1\rangle && (2.27)\\ &= \frac{1}{2} && (2.28) \end{aligned}$$

for the $|+\rangle$ state. The same probabilities hold for the $|-\rangle$ state. Again, the state will be destroyed on measurement and be either $|0\rangle$ or $|1\rangle$ afterward, depending on the measurement outcome.

A qubit represents the smallest possible quantum system. The stochastic nature of quantum physics allows a qubit to be in a superposition of the two computational basis states $|0\rangle$ and $|1\rangle$. Nevertheless, it is impossible to access such a superposition state directly.

The next section will describe how combining multiple qubits into a bigger quantum system gives rise to an exponential growth of the state vector of such systems and how multiple qubits can be *entangled* with each other.

2.2 Multiple Qubits and Entanglement

The state vector of a single qubit lies in a two dimensional space, assigning a complex-valued amplitude to each of the both possible measurement outcomes $|0\rangle$ and $|1\rangle$. The state vector of a multi qubit system is defined by the *tensor product* of the state vectors of the individual subsystems. For a two qubit system consisting of $|\psi_1\rangle = \alpha_1 |0\rangle + \beta_1 |1\rangle$ and $|\psi_2\rangle = \alpha_2 |0\rangle + \beta_2 |1\rangle$ the state vector is given by:

$$
\begin{aligned}
|\psi_{1,2}\rangle &= |\psi_1\rangle \otimes |\psi_2\rangle && (2.29)\\
&= (\alpha_1 |0\rangle + \beta_1 |1\rangle) \otimes (\alpha_2 |0\rangle + \beta_2 |1\rangle) && (2.30)\\
&= \alpha_1\alpha_2 |0\rangle |0\rangle + \alpha_1\beta_2 |0\rangle |1\rangle + \beta_1\alpha_2 |1\rangle |1\rangle + \beta_1\beta_2 |1\rangle |1\rangle && (2.31)\\
&= \alpha_1\alpha_2 |00\rangle + \alpha_1\beta_2 |01\rangle + \beta_1\alpha_2 |10\rangle + \beta_1\beta_2 |11\rangle && (2.32)\\
&= \alpha_1\alpha_2 |0\rangle + \alpha_1\beta_2 |1\rangle + \beta_1\alpha_2 |2\rangle + \beta_1\beta_2 |3\rangle , && (2.33)
\end{aligned}
$$

where we define $|0\rangle = |00\rangle$, $|1\rangle = |01\rangle$, $|2\rangle = |10\rangle$ and $|3\rangle = |11\rangle$. In the general case, the wave function of a n-qudit system is given by a 2^n dimensional vector:

$$|\psi\rangle = \sum_{i=0}^{2^n} a_i |i\rangle . \tag{2.34}$$

Therefore, a classical simulation of a n-dimensional qudit system has to keep track of 2^n complex amplitudes. This makes it impossible to simulate quantum systems above a certain size. For the classical simulation of a system consisting of 500 qubits, the state vector's dimension is already larger than the number of atoms in the universe.

As in the single qubit case, the probability to observe state $|n\rangle$ is given by a_n^2. It is also possible to only measure a subset of the qubits, leaving the other qubits in the normalized state

$$|\psi\prime\rangle = \frac{(M_m \otimes I) |\psi\rangle}{\sqrt{p(m)}}. \tag{2.35}$$

An interesting property that can appear in multi-qudit systems is *entanglement*. Consider for instance the two-qudit state

$$|\psi\rangle = \frac{|00\rangle + |11\rangle}{\sqrt{2}}, \tag{2.36}$$

which can be created with a very simplistic quantum program as shown later in section **??**. Note that this state is a proper two-qubit state as it fulfills the normalization property $a_{00}^2 + a_{11}^2 = \frac{1}{\sqrt{2}}^2 + \frac{1}{\sqrt{2}}^2 = \frac{1}{2} + \frac{1}{2} = 1$.

Nevertheless, there are no two single-qubit states $|a\rangle$ and $|b\rangle$ such that $|\psi\rangle = |a\rangle |b\rangle$. The two qubits of $|\psi\rangle$ are *entangled* with each other. Measuring one of

the qubits immediately determines the state of the other qubit, i.e. measuring the first qubit as $|0\rangle$ happens with probability

$$p_1(0) = \langle\psi| (M_0 \otimes I)^\dagger (M_o \otimes I) |\psi\rangle \tag{2.37}$$
$$= \frac{1}{\sqrt{2}} \langle 00| \frac{1}{\sqrt{2}} |00\rangle \tag{2.38}$$
$$= \frac{1}{2}, \tag{2.39}$$

leaving the system in the post-measurement state

$$|\psi\prime\rangle = \frac{(M_0 \otimes I)\psi}{\sqrt{p_1(0)}} \tag{2.40}$$
$$= \frac{\frac{1}{\sqrt{2}} |00\rangle}{\frac{1}{\sqrt{2}}} \tag{2.41}$$
$$= |00\rangle . \tag{2.42}$$

The same maths apply for the case of measuring the first qubit as $|1\rangle$.

Even if the state of the second qubit is not determined before, it will be either $|0\rangle$ or $|1\rangle$ from the moment on the *other* qubit has been measured. The exponential growth of the state space dimension and entanglement are two important properties of quantum systems which make them hard to simulate classically. Known quantum algorithms with quantum speedups like Shor's algorithm create entanglement in smart ways to perform calculations in ways which seem to be impossible for classical computers.

The next section introduces the notion of *quantum gates* which allow to manipulate the state of a single or multiple qubits.

2.3 Quantum Gates

It is physically possible to modify the state vector of a quantum system even when it is in a coherent state. This opens the theoretical possibility to perform calculations with them and build quantum computers.

Modifications happen by the application of so-called *quantum gates* to the state. Quantum physics allows the gates only to be linear and reversible. Thus, quantum gates can be mathematically described as unitary matrices. Gates vary in the number of qubits on which they act and the effects they have on the qubits' state.

This chapter will introduce single and multi-qubit gates and gives an overview over some basic quantum operations.

2.3.1 Single-Qubit Gates

Single qubit gates are linear mappings that can be applied to the state vector of a single qubit. Mathematically, single-qubit gates can be described by 2×2 unitary matrices. The fact that these matrices are unitary makes sure the state $|\phi\rangle = G|\psi\rangle$ after gate G has been applied to state $|\psi\rangle$ is a proper quantum state which preserves the normalization constraint $\alpha_{|\phi\rangle}^2 + \beta_{|\phi\rangle}^2 = 1$.

An example of a single qubit gate is the NOT or X gate, also denoted as:

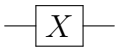

or

The X gate is the quantum analog of the classical NOT gate. Like the classical version, the X gate swaps the states $|0\rangle$ and $|1\rangle$ when applied to them. It is even more general though, as it maps a single-qubit state of the form

$$|\psi\rangle = \alpha|0\rangle + \beta|1\rangle \tag{2.43}$$

to the state

$$|\phi\rangle = \beta|0\rangle + \alpha|1\rangle \tag{2.44}$$

thus swapping the amplitudes for $|0\rangle$ and $|1\rangle$. The X gate has the following matrix representation:

$$X = \begin{pmatrix} 0 & 1 \\ 1 & 0 \end{pmatrix}. \tag{2.45}$$

A single qubit gate is applied to a quantum state by matrix multiplication:

$$\begin{aligned} |\phi\rangle &= X|\psi\rangle && (2.46)\\ &= \begin{pmatrix} 0 & 1 \\ 1 & 0 \end{pmatrix}|\psi\rangle && (2.47)\\ &= \begin{pmatrix} 0 & 1 \\ 1 & 0 \end{pmatrix}\begin{pmatrix} \alpha \\ \beta \end{pmatrix} && (2.48)\\ &= \begin{pmatrix} \beta \\ \alpha \end{pmatrix} && (2.49) \end{aligned}$$

Another example for a single qubit gate with no classical analog is the *Hadamard gate* or H gate, described by the unitary:

$$H = \frac{1}{\sqrt{2}}\begin{pmatrix} 1 & 1 \\ 1 & -1 \end{pmatrix}, \tag{2.50}$$

Notice that the H gate is a unitary as it is reversible:

$$H^\dagger H = I. \tag{2.51}$$

The Hadamard gate maps between the so called Z and X bases, mapping the states:

$$H\left|0\right\rangle = \left|+\right\rangle \tag{2.52}$$
$$H\left|1\right\rangle = \left|-\right\rangle \tag{2.53}$$

and back

$$H\left|+\right\rangle = \left|0\right\rangle \tag{2.54}$$
$$H\left|-\right\rangle = \left|1\right\rangle. \tag{2.55}$$

The Hadamard gate is a good example of how the Bloch Sphere visualization can help understand a qubit state's transformation. The application of the Hadamard gate to the $|+\rangle$ is shown in figure **??**.

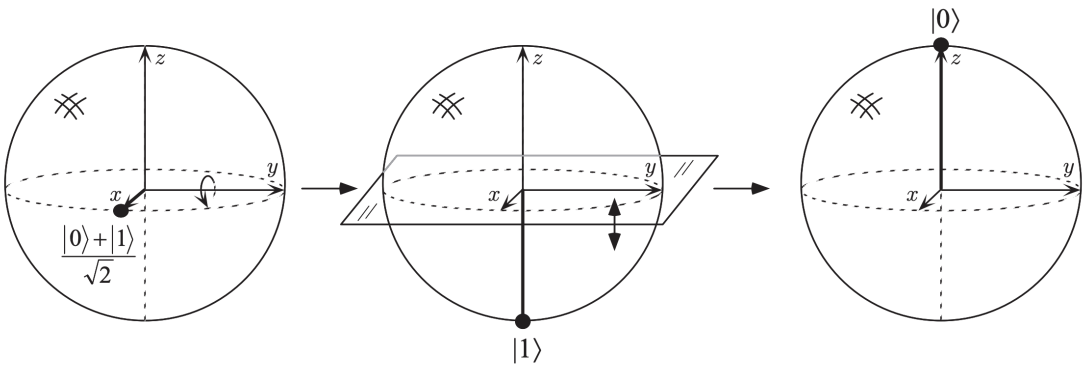

Figure 2.2: Visualization of the Hadamard gate on the Bloch sphere, acting on the $|+\rangle$ state [**?**].

An overview of some common single-qubit gates is given in figure **??**.

Operator	Gate	Matrix
X		$\begin{pmatrix} 0 & 1 \\ 1 & 0 \end{pmatrix}$
Y		$\begin{pmatrix} 0 & -i \\ i & 0 \end{pmatrix}$
Z		$\begin{pmatrix} 1 & 0 \\ 0 & -1 \end{pmatrix}$
H		$\frac{1}{\sqrt{2}} \begin{pmatrix} 1 & 1 \\ 1 & -1 \end{pmatrix}$
S		$\begin{pmatrix} 1 & 0 \\ 0 & i \end{pmatrix}$
T		$\begin{pmatrix} 1 & 0 \\ 0 & e^{i\frac{\pi}{2}} \end{pmatrix}$

Table 2.1: Overview of common single-qubit gates.

Though there are indefinitely many possible quantum gates in theory, a universal finite gate set consisting of only a few gates is sufficient to construct arbitrary unitary transformations. This is the same as in the classical case where NAND gates suffice to build up arbitrary classical computation circuits and good news for the fabrication of quantum computers with reusable components.

However, single-qubit gates are not sufficient to build all possible unitary transformations on multi-qubit systems. For this purpose, multi-qubit gates are a necessity.

2.3.2 Multi-Qubit Gates

Single qubit gates are not enough to create universal gate sets for quantum computation. In order to run arbitrary quantum programs *controlled* gates are needed. Controlled quantum gates are simple extensions of single-qubit gates. Every single-qubit gate can be implemented as a controlled version of it with one *control* and one *target* qubit. Only if the control qubit is in the $|1\rangle$ state, the gate is applied to the target qubit. As the control qubit can be in a superposition state, it is possible to apply and not apply the gate to the target qubit at the same time, so to say.

The prototypical two qubit gate is the controlled NOT or CNOT gate. It is the controlled version of the X gate described before. As the CNOT gate acts on

a two qubit state, it can be described by a 4×4 unitary matrix. Each column describes the mapping of one of the four base state $|00\rangle$, $|01\rangle$, $|10\rangle$ and $|11\rangle$. The matrix representation of the CNOT gate is the following:

$$CNOT = \begin{pmatrix} 1 & 0 & 0 & 0 \\ 0 & 1 & 0 & 0 \\ 0 & 0 & 0 & 1 \\ 0 & 0 & 1 & 0 \end{pmatrix}. \tag{2.56}$$

The matrix can be read as follows: The first two columns describe that the vectors $|00\rangle$ and $|01\rangle$ will not change when the gate is applied to these states. Only when the first qubit is in the $|1\rangle$ state will the state of the second qubit be swapped. Thus $|10\rangle$ will be mapped to $|11\rangle$ and $|11\rangle$ to $|10\rangle$.

This also shows how the matrix representation of generalized two-qubit gates can be derived: As long as the control qubit is off, it does not affect the state. Thus, the controlled gate matrix is the same as the identity with 1s on the diagonal and 0s elsewhere in the upper left corner. Only when the first qubit is in the $|1\rangle$ state, the matrix differs from the identity. For example, the controlled version of the Z gate

$$Z = \begin{pmatrix} 1 & 0 \\ 0 & -1 \end{pmatrix} \tag{2.57}$$

is given by:

$$CZ = \begin{pmatrix} 1 & 0 & 0 & 0 \\ 0 & 1 & 0 & 0 \\ 0 & 0 & 1 & 0 \\ 0 & 0 & 0 & -1 \end{pmatrix}. \tag{2.58}$$

Controlled gates are represented with a vertical line ending in a black dot indicating the control qubit:

With two-qubit operations at hand, it is possible to build a universal gate set. A commonly used gate set is the so-called *Clifford + T* set, consists of the gates $CNOT$, H, S and T. The Solovay-Kitaev theorem guarantees that this set can efficiently approximate any unitary operation. In this study, another universal gate set will be used, though, composed of the CZ, $\sqrt{X}$, $\sqrt{Y}$ and T gates.

The next sections will demonstrate how gates can be composed into *quantum circuits*, a notation for quantum programs.

2.4 Quantum Circuits

The standard model for computation in theoretical computer science is the Turing Machine. Invented by Alan Turing in 1936 during World War Two, it is a powerful tool to understand the limits of (classical) computation. The theoretical nature of the Turing machine gives it unlimited computational resources like memory though, which do not reflect the properties of realizable computer architectures.

Another computation model that does not suffer from this gap between theory and practical devices is the *circuit model*. In the classical circuit model, each bit is represented by a wire, and operations (or gates) are represented by different shapes acting on those wires. The circuit model is as powerful as a Turing Machine and the model of choice in quantum computing.

Quantum programs are described by quantum circuits. As in the classical case, each qubit is represented by a wire and each gate by a rectangular on those wires. Figure **??** describes a very simple quantum circuit which flips a single qubit starting in the $|0\rangle$ state by applying a X gate before measuring it.

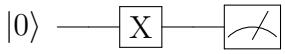

Figure 2.3: A simple quantum circuit applying an X gate to a qubit initialized in the $|0\rangle$ state before measuring it.

The circuit is being read from left to right. Important to note though is that for the calculation of the resulting state, the matrix representation of the gates are multiplied from the left side to the current state by simply following the rules of linear algebra. In the example above the final state of the program represented at the end of the circuit is:

$$
\begin{aligned}
|\phi\rangle &= X\,|\psi\rangle && (2.59)\\
&= \begin{pmatrix} 0 & 1 \\ 1 & 0 \end{pmatrix} |\psi\rangle && (2.60)\\
&= \begin{pmatrix} 0 & 1 \\ 1 & 0 \end{pmatrix} \begin{pmatrix} \alpha \\ \beta \end{pmatrix} && (2.61)\\
&= \begin{pmatrix} \beta \\ \alpha \end{pmatrix}. && (2.62)
\end{aligned}
$$

In practice, circuits will consist of several qubits and multiple gates applied to them. It is possible to apply gates to different qubits sequentially as well as in parallel, as demonstrated in figure **??**:

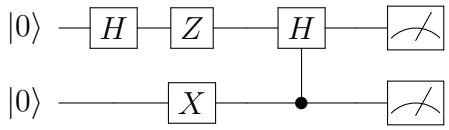

Figure 2.4: A quantum circuit acting on two qubits. The effect of parallel applications of single-qubit gates is defined by the tensor product of the gates.

Note that when calculating the state of the quantum program above, one has to build the tensor product of all qubit states to calculate the state of the system. For the circuit from figure **??**, the initial state before any gate has been applied is:

$$|\psi_{init}\rangle = |0\rangle \otimes |0\rangle \tag{2.63}$$
$$= \begin{pmatrix} 1 \\ 0 \end{pmatrix} \otimes \begin{pmatrix} 1 \\ 0 \end{pmatrix} \tag{2.64}$$
$$= \begin{pmatrix} 1 \\ 0 \\ 0 \\ 0 \end{pmatrix} \tag{2.65}$$
$$= |00\rangle \tag{2.66}$$

When a gate gets applied to only a subset of the qubits as in the case of the first H gate in the circuit above, the unitary applied to the multi-qubit state is implicitly the tensor product of the gate on that qubit and identity matrices on the remaining qubits. For the given circuit, the state $|\psi_{H_1}\rangle$ after the first H gate on the first qubit is calculated as:

$$
\begin{aligned}
|\psi_{H_1}\rangle &= (H \otimes I)\,|00\rangle && (2.67)\\
&= \left(\frac{1}{\sqrt{2}}\begin{pmatrix}1 & 1\\ 1 & -1\end{pmatrix} \otimes \begin{pmatrix}1 & 0\\ 0 & 1\end{pmatrix}\right)|00\rangle && (2.68)\\
&= \frac{1}{\sqrt{2}}\begin{pmatrix}1 & 0 & 1 & 0\\ 0 & 1 & 0 & 1\\ 1 & 0 & -1 & 0\\ 0 & 1 & 0 & -1\end{pmatrix}|00\rangle && (2.69)\\
&= \frac{1}{\sqrt{2}}\begin{pmatrix}1 & 0 & 1 & 0\\ 0 & 1 & 0 & 1\\ 1 & 0 & -1 & 0\\ 0 & 1 & 0 & -1\end{pmatrix}\begin{pmatrix}1\\ 0\\ 0\\ 0\end{pmatrix} && (2.70)\\
&= \frac{1}{\sqrt{2}}\begin{pmatrix}1\\ 0\\ 1\\ 0\end{pmatrix} && (2.71)\\
&= |+0\rangle\,. && (2.72)
\end{aligned}
$$

This corresponds to the intuition that after applying a H gate to the first qubit, it should be in the $|+\rangle$ state while the second qubit remains in the $|0\rangle$ state.

Similar as for the first gate, the unitary applied to the state when multiple gates are applied to different qubits at the same time, is constructed by the tensor product of those gates. The state $|\psi_{Z_1X_2}\rangle$ after the Z gate is applied to first and the X gate is applied to the second qubit is calculated as:

$$
\begin{aligned}
|\psi_{Z_1X_2}\rangle &= (Z \otimes X)\,|+0\rangle && (2.73)\\
&= \left(\begin{pmatrix}1 & 0\\ 0 & -1\end{pmatrix} \otimes \begin{pmatrix}0 & 1\\ 1 & 0\end{pmatrix}\right)|+0\rangle && (2.74)\\
&= \begin{pmatrix}0 & 1 & 0 & 0\\ 1 & 0 & 0 & 0\\ 0 & 0 & 0 & -1\\ 0 & 0 & -1 & 0\end{pmatrix}|+0\rangle && (2.75)\\
&= \begin{pmatrix}0 & 1 & 0 & 0\\ 1 & 0 & 0 & 0\\ 0 & 0 & 0 & -1\\ 0 & 0 & -1 & 0\end{pmatrix}\begin{pmatrix}\frac{1}{\sqrt{2}}\\ 0\\ \frac{1}{\sqrt{2}}\\ 0\end{pmatrix} && (2.76)\\
&= \begin{pmatrix}0\\ \frac{1}{\sqrt{2}}\\ 0\\ -\frac{1}{\sqrt{2}}\end{pmatrix} && (2.77)\\
&= |-1\rangle\,. && (2.78)
\end{aligned}
$$

This again matches with the intuition that applying a Z gate to the $|+\rangle$ state leaves the first qubit in the $|-\rangle$ state, and the X gate on the second qubit moves it from the $|0\rangle$ to the $|1\rangle$ state.

The final state $|\psi_{final}\rangle$ of the circuit is calculated by applying the 4×4 matrix representation of the controlled H gate to $|-1\rangle$. Notice that the second qubit is the controlled qubit in this case:

$$|\psi_{final}\rangle = CH\,|-1\rangle \tag{2.79}$$

$$= \begin{pmatrix} 1 & 0 & 0 & 0 \\ 0 & \frac{1}{\sqrt{2}} & 0 & \frac{1}{\sqrt{2}} \\ 0 & 0 & 1 & 0 \\ 0 & \frac{1}{\sqrt{2}} & 0 & -\frac{1}{\sqrt{2}} \end{pmatrix} |-1\rangle \tag{2.80}$$

$$= \begin{pmatrix} 1 & 0 & 0 & 0 \\ 0 & \frac{1}{\sqrt{2}} & 0 & \frac{1}{\sqrt{2}} \\ 0 & 0 & 1 & 0 \\ 0 & \frac{1}{\sqrt{2}} & 0 & -\frac{1}{\sqrt{2}} \end{pmatrix} \begin{pmatrix} 0 \\ \frac{1}{\sqrt{2}} \\ 0 \\ -\frac{1}{\sqrt{2}} \end{pmatrix} \tag{2.81}$$

$$= \begin{pmatrix} 0 \\ 0 \\ 0 \\ 1 \end{pmatrix} \tag{2.82}$$

$$= |11\rangle\,. \tag{2.83}$$

The first qubit has been swapped from the $|-\rangle$ to the $|1\rangle$ state as the second qubit is in the $|1\rangle$ state and the H gate has been applied. The circuit **??** thus maps the initial state $|00\rangle$ to $|11\rangle$.

Another simple quantum circuit with interesting properties is shown in figure **??**.

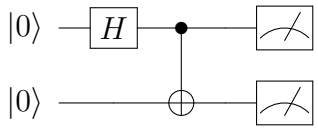

Figure 2.5: A quantum circuit to create maximally entangled 2-qubit states.

The Hadamard gate on the first qubit maps the system from the initial $|00\rangle$ into the $|+0\rangle$ state. Afterward, the first qubit, which is currently between the $|0\rangle$ and $|1\rangle$ state on the Bloch Sphere, is used as the control qubit in the $CNOT$ gate. This has an interesting effect on the second qubit as the X gate is applied and not applied at the same time to it, entangling the two qubits with each other. The final state before measurement is then $\frac{|00\rangle+|11\rangle}{2}$ which has already been discussed in section **??**. The state is also known as one of the four *Bell states*, which represent maximally entangled two-qubit states and which play an important role in the analysis of *quantum communication*.

This simple quantum circuit demonstrates how entanglement can be created by applying controlled gates with qubits in superposition states. Entanglement plays an essential role in the construction of so-called random quantum circuits in recent quantum supremacy experiments. These kinds of circuits will be discussed in chapter **??** after a short overview of the theoretical computational power of

quantum computers.

2.5 Quantum Computational Complexity

It is essential to understand the theoretical capabilities and limitations of quantum computers to understand for which kind of problems they provide advantages over classical computers. For many years, it has been assumed that the extended Church Turing thesis, stating that a probabilistic Turing machine can efficiently simulate any realistic model of computation, holds. This thesis is challenged by quantum computers, potentially solving specific problems exponentially faster than classical computers.

The class of problems which can be solved efficiently by a quantum computer is called **BQP**, shorthand for *bounded-error quantum polynomial time*. A decision problem is in **BQP** if there exists a quantum program that solves the decision problem in 2/3 of the cases and runs in polynomial time. This is the quantum analog of the *bounded-error probabilistic polynomial time* or **BPP** which is decidable by a probabilistic Turing machine in polynomial time and believed to be the same as **P**.

Currently, there are only a few problems known to be in **BQP**, which are suspected not to be in **P**, providing evidence for the superiority of quantum computers. One of these problems is *factorization*, the problem of decomposing a composite integer into its prime factors. This problem has been known to be in *NP* before. Though, it is also known that factorization is not an **NP**-hard problem, indicating that quantum computers are probably not able to provide an exponential speedup for every problem that is not efficiently solvable on a classical computer. Indeed, classical algorithms might even exist, which can solve factorization on a classical computer efficiently, which have not been discovered yet.

While **BQP** seems to include **P** and intersect with **NP**, it can be shown that it is strictly included in **PSPACE**. The relationship of these complexity classes is visualized in figure **??**.

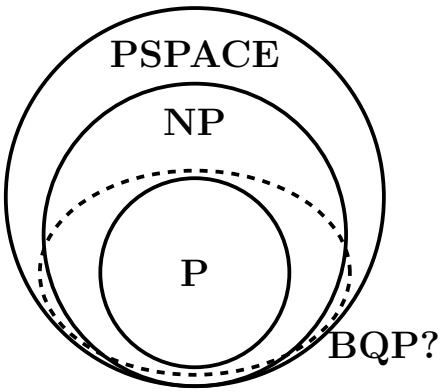

Figure 2.6: Relation of Complexity Classes to each other.

While it is hard to prove some fundamental relationships between complexity classes like the famous $\mathbf{P} \stackrel{?}{=} \mathbf{NP}$ problem, it is believed that quantum computers can solve specific problems with practical applications like integer factorization or the simulation of quantum systems exponentially faster than classical computers.

The moment in time a physical quantum computer can outperform a classical computer on a specific problem for the first time has been coined by John Preskill in 2012 as *quantum supremacy*. Recently, Google announced their quantum supremacy results with a 54 qubit quantum computer, further challenging the extended Church Turing thesis and providing the first physical evidence that it might be possible to build quantum computers with advantages over classical computers.

3 Random Circuit Sampling

Despite four decades of research in quantum computing, there was no physical proof of whether it would be possible to realize quantum computers that have an advantage over classical ones. This only changed recently, when a team from Google and the UCSB claimed to have demonstrated *quantum supremacy* with a 54 superconducting qubit quantum processor [**?**]. For this purpose, they chose the problem of *random circuit sampling*, a problem designed explicitly as a quantum supremacy experiment [**?**].

This chapter will motivate and introduce the theoretical framework of random circuit sampling, also used as the benchmark for Restricted Boltzmann Machines in this study. Further, the results of Google's quantum supremacy experiments and their implications for the (near) future of quantum computing will be discussed.

3.1 Quantum Supremacy

John Preskill has coined the term *quantum supremacy* in 2012 [**?**]. It describes the point in time when a physical quantum computer outperforms a classical computer on some task for the first time. The problem solved by the quantum computer does not need to be useful. Its only purpose is to prove that a quantum computer can be realized, which has an advantage over classical computers on *some* problem.

There exist different proposals for quantum supremacy experiments. Since quantum computers do not promise to outperform classical computers on every problem, as discussed in section **??**, but only provide a practical advantage for problems which lie in **BQP** and outside of **P**, quantum supremacy experiments must be based upon a strong theoretical foundation.

One way to demonstrate quantum supremacy would be to run Shor's algorithm for integer factorization [**?**] on a physical quantum computer on some number which would not be feasible to decompose with known classical algorithms on existing supercomputers. The issue with this approach is that many qubits are necessary to represent such numbers while today it is possible to build quantum processors with about 50 qubits of reasonable quality.

Another famous proposal for a quantum supremacy experiment is *Boson Sampling*, which is based on the fact that calculating the permutant of a matrix is computationally hard [**?**].

The approach that a team from Google and UCSB took last year is called *Random Circuit Sampling* (RCS). In this approach, random quantum circuits

of specific structures that create highly entangled states are run on a quantum processor and are simulated classically. For enough qubits and depth, performing the classical simulations would take years on the biggest existing supercomputers. If the quantum computer can generate outputs for such circuits which cannot be simulated classically anymore while their output can still be verified to be correct, this would demonstrate quantum supremacy.

A metric that allows the verification on random circuit instances that cannot be simulated is the *cross entropy fidelity*.

3.2 Cross Entropy Fidelity

The challenge of quantum supremacy is that one has to be able to verify the results of the quantum computer on instances which cannot be calculated classically anymore. In the case of integer factorization, this is a simple task as the test for the correctness consists of simple multiplications which can be performed efficiently. Since integer factorization needs more qubits than currently available in existing quantum computer hardware, other supremacy experiments like RCS provide a framework to demonstrate quantum supremacy much earlier.

The first observation to understand the concept of RCS is that every quantum circuit acting on n qubits can be described by a single 2^n dimensional unitary matrix, as illustrated in figure **??**. This follows from the fact that quantum gates are described by unitary transformations and the matrix product, as well as the tensor product of two unitaries, is a unitary again.

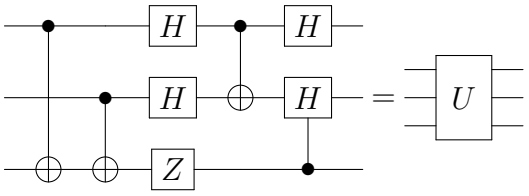

(3.1)

Figure 3.1: Every Circuit can be described by one big unitary acting on n qubits. W.l.o.g. the resulting states corresponds to the first row of the unitary U.

A quantum circuit consisting of gates chosen uniformly at random thus will act like a uniformly random unitary U. Since the input state of the circuit can be assumed to be initialized in the $|0\rangle^{\otimes n}$ state, the amplitudes of the final quantum state of the circuit correspond to the first column of the random unitary U.

This column's entries are complex numbers with real and imaginary parts distributed by an unbiased Gaussian with respect to the normalization constraints. The output probabilities of the random circuit are given by the squared norms of these entries. They are thus distributed as the square of a Gaussian distribution which is an exponential distribution, also known as a Porter-Thomas distribution

[**?**]. So the probabilities $p(x_j) = |\langle x_j | \psi_{RC} \rangle|^2$ to observe bitstrings $x_j \in \{x_j\}_{j=1}^N$ with $N = 2^n$ are distributed according to

$$Pr(p) = e^{-Np} \tag{3.2}$$

as visualized in figure **??**.

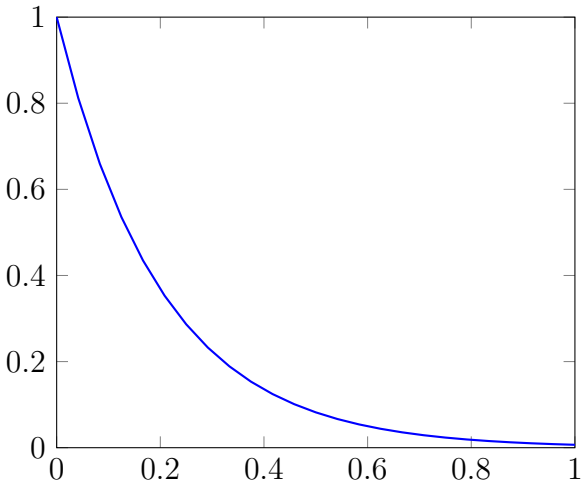

Figure 3.2: Distribution $P(p_{x_j})$ of output probabilities p_{x_j} of a quantum circuit. The distribution $P(p_{x_j}) = e^{-Np}$ is distributed as Porter Thomas. A lot of output strings will have a low probability to be observed and a few output strings will dominate the observed outputs [**?**].

As quantum computers suffer from decoherent noise, it is important to understand how noise during the computation influences the output distribution from the quantum computer and if noisy quantum computers can still outperform classical computers on the RCS task. Knowing that the outputs are Porter Thomas distributed will help with that.

The task is to understand how samples $S = \{x_1, \ldots, x_m\}$ drawn from a perfect execution of U compare to a set $S' = \{x'_1, \ldots, x'_m\}$ of samples drawn from a potentially noisy execution of U.

A well motivated measure for the difference between the underlying probability distributions p_U and p'_U of samples S and S' is the *cross entropy*, defined as

$$H(p'_U, p_U) = -\sum_{j=1}^{N} p'_U(x_j|U) \log p_U(x_j). \tag{3.3}$$

Of interest is the expected quality of the potentially noisy execution over different random circuit instances:

$$\mathbb{E}_U[H(p'_U, p_U)] = \mathbb{E}\left[\sum_{j=1}^{N} p'_U(x_j|U) \log \frac{1}{p_U(x_j)}\right]. \tag{3.4}$$

The output of the noisy execution can be assumed to be statistically uncorrelated with the output of the perfect execution. Thus, and since the output distribution for a fixed x_j over many random circuit instances U also has the shape of the Porter-Thomas distribution [**?**], $-\mathbb{E}_U[\log p_U(x_j)]$ can be computed independently as

$$-\mathbb{E}_U[\log p_U(x_j)] \approx -\int_0^\infty N e^{-NP} \log p \, dp \tag{3.5}$$

$$= \log N + \gamma, \tag{3.6}$$

where $\gamma \approx 0.577$ is the Euler constant. Using the fact that $\sum_{j=1}^{N} p'_U(x_j) = 1$ for any distribution $p_U\prime$, the average cross entropy $\mathbb{E}_\mathbb{U}[H(p'_U, p_U)]$ between the Porter-Thomas distribution and any other uncorrelated distribution is given as

$$\mathbb{E}_U[H(p'_U, p_U)] = \log N + \gamma. \tag{3.7}$$

This is equivalent to the cross entropy $H_0 = \log N + \gamma$ between the Porter-Thomas and the uniform distribution. Thus, on average, a worst-case noisy execution will be as good compared to a perfect execution as sampling every bitstring with probability $1/N$. H_0 differs from the entropy $H(p_U)$ of the Porter-Thomas distribution, which corresponds to the cross entropy with itself, only by a -1 term:

$$H(p_U) = -\int p N^2 e^{-Np} \log p \, dp \tag{3.8}$$

$$= \log N - 1 + \gamma, \tag{3.9}$$

This directly leads to a benchmark for any algorithm A_U sampling output strings from a random circuit U, given either by a classical simulation or by a (noisy) quantum computer. The quality of A_U can be calculated as the difference between the entropy of the uniform distribution and the cross entropy of the output samples from A_U with the Porter-Thomas distribution. This metric is defined as the *cross entropy difference* [**?**]:

$$\Delta H(p_A) \equiv H_0 - H(p_A, p_U) \tag{3.10}$$

$$= \sum_j \left(\frac{1}{N} - p_A(x_j|U)\right) \log \frac{1}{p_U(x_j)}. \tag{3.11}$$

The cross entropy difference is zero for an algorithm sampling from the uniform distribution and one for an algorithm sampling from the underlying Porter-Thomas distribution of the circuit.

Notice that in order to calculate $\Delta H(p_A)$, a perfect simulation of the random circuit is necessary as the values of $p_U(x_j)$ have to be known. This is not possible in the quantum supremacy regime. As discussed shortly, it will be possible to

extrapolate the cross entropy difference $\Delta H(p_A)$ of A_U to the quantum supremacy regime with high precision based on samples of its cross entropy difference on smaller circuit instances which can still be simulated classically.

Another justification for the cross entropy difference is that the l_1 distance between the uniform and Porter Thomas distribution

$$l_1(p,q) = \|p-q\|_1 \tag{3.12}$$

$$= \sum_{j=1}^{N} \mid p_i - q_i \mid \tag{3.13}$$

is a constant and thus independent of the number of qubits n. Therefore a constant number of samples is sufficient to calculate the cross entropy difference.

The experimental cross entropy difference

$$\alpha = \mathbb{E}_U[\Delta H(p'_U)] \tag{3.14}$$

can be obtained by the execution of several random circuits U. Quantum supremacy is achieved by a physical quantum computer when its average cross entropy

$$1 \geq \alpha > C \tag{3.15}$$

is greater than the average performance C of the best known classical algorithm A^*:

$$C = \mathbb{E}_U[\Delta H(p^*)]. \tag{3.16}$$

In the regime where perfect simulations are possible, $C = 1$ and quantum supremacy cannot be achieved. For sufficiently many qubits, perfect simulations will not be possible anymore and $1 > C \geq 0$ with C decreasing exponentially with the number of gates $g >> n$. For a typical set of samples S_{exp} drawn from the execution of a quantum circuit, the central limit theorem implies that

$$\alpha \simeq H_0 - \frac{1}{m}\sum_{j=1}^{m} \log \frac{1}{p_U(x_j^{exp})}. \tag{3.17}$$

The experimental setup to estimate the cross entropy difference of any approximate simulation of a quantum computer thus is:

1. Select random circuit U.
2. Take sufficiently many samples $S_{exp} = \{x_1, \ldots, x_m\}$, m in range $10^3 - 10^6$.
3. Compute the quantities $\log \frac{1}{p_U(x_j^{exp})}$ with the aid of a sufficiently large quantum computer.

4. estimate α using equation **??**.

3.3 Extrapolating to the Supremacy Regime

Keeping the qubits in a coherent state during a calculation and applying quantum gates exactly is a difficult task. Qubits will suffer from decoherent noise, which will destroy the quantum states. This will happen in particular in the early implementations of quantum computers.

Before large scale error-corrected quantum computers will be available, so-called noisy intermediate-scale quantum (NISQ) computers present the first stage of quantum computing hardware. Such noisy devices will already provide an advantage over classical computers on specific problems. If the noise can be kept below a certain threshold, a NISQ device can demonstrate quantum supremacy on the RCS task.

In the presence of noise, the quantum state ρ generated by a physical quantum computer after the execution of a random circuit U can be represented as

$$\rho = \tilde{\alpha} U \left|\psi_0\right\rangle \left\langle\psi_0\right| U^\dagger + (1-\tilde{\alpha})\sigma \tag{3.18}$$

with $\tilde{\alpha}$ being the circuit *fidelity* and noise term σ being an orthogonal state to the true state $\left\langle\psi_0\right| U^\dagger \sigma U \left|\psi_0\right\rangle = 0$. The corresponding average cross entropy difference then is:

$$\alpha = \mathbb{E}_U[H_0 + \sum_j \left\langle x_j\right| \rho \left|x_j\right\rangle \log p_U(x_j)] \tag{3.19}$$

$$= \tilde{\alpha} + (1-\tilde{\alpha})H_0 + \mathbb{E}_U\left[(1-\tilde{\alpha})\sum_j \left\langle x_j\right| \sigma \left|x_j\right\rangle \log p_U(x_j)\right]. \tag{3.20}$$

The states generated by the random circuits are maximally entangled. A single bit or phase flip introduced by an additional X or Z gate in the circuit completely destroys such a state. Instead of being Porter Thomas distributed, the output with an additional X or Z gate at any position would be almost uniformly distributed, as shown in figure **??**.

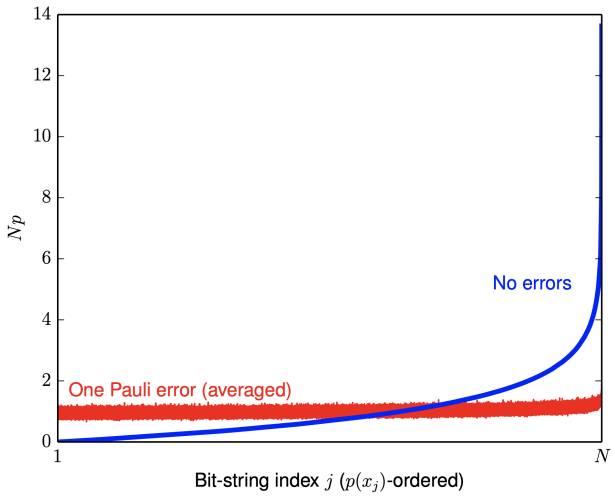

Figure 3.3: Blue: Output bitstrings of a random circuit ordered by their probabilities. Red: Averaged simulated output distribution with one Pauli error on all possible positions in a 5×4 qubits random circuit with depth 40. The distribution is almost uniform and almost uncorrelated with the real output distribution. The small tild at the end can be explained by the fact that Z gates close to the end of the circuit do not have an effect on the output distribution [**?**].

In other words, it is not possible to infer any information about the output probabilities without a perfect simulation of the circuit. This justifies the assumption that the actual output probabilities and the output of the quantum computer are (almost) uncorrelated. This assumption of no correlation, in turn, leads to the conclusion that the circuit fidelity $\tilde{\alpha}$ of a random circuit U is approximately equal to the average cross entropy

$$\alpha = \mathbb{E}_U[\Delta H(p_{exp})] \approx \tilde{\alpha}. \tag{3.21}$$

This means that the fidelity α of a quantum device can be extrapolated to the quantum supremacy regime with estimates of it on random circuit instances which can still be simulated classically.

Even further, this also means that the cross entropy difference can also aid to estimate the single and two qubit gate and errors of a quantum device:

$$\alpha \approx e^{-r_1 g_1 - r_2 g_2 - r_{init} n - r_{mes} n} \tag{3.22}$$

with $r_1, r_2 \ll 1$ being the Pauli error rates for 1 and 2 qubit gates, $r_{init}, r_{mes} \ll 1$ the initialisation and measurement error and $g_1, g_2 \gg 1$ being the numbers of 1 and 2 qubit gates. This relation has been numerically confirmed by Boixo et al. [**?**], indicating that the relation between the cross entropy difference and the circuit fidelity can be used to extrapolate the cross entropy difference of a quantum device

to the quantum supremacy regime.

So, even with a noisy quantum computer, it is possible to demonstrate quantum supremacy, i.e., to approximate the output distribution of random circuit instances better than possible by any classical algorithm known, by calculating the fidelity on random circuit instances still possible to simulate classically and extrapolating it to the supremacy regime using equation **??**. If the fidelity is greater zero in the regime where no classical simulation is possible anymore, quantum supremacy has been demonstrated.

3.4 Random Circuit Design

The derivation of the cross entropy difference based on the assumption that the output probabilities of random circuit instances will be distributed according to the Porter-Thomas distribution. As it is known that circuits of low depth as well as so-called *Clifford Circuits* can be simulated classically efficiently, it is crucial to understand which requirements the structures of the random circuits has to fulfill in order to be hard to simulate classically and generate exponential output distributions.

In a fully connected architecture, random circuits approximate a pseudo-random distribution with logarithmic depth. Fully connected in this statement means that 2-qubit gates can be applied to pairs of any two qubits of the circuit. In architectures like superconducting qubits such as Google's Sycamore processor, the qubits are laid out on a 2D lattice, allowing 2-qubit gates only to be applied to neighboring qubits on that lattice. Circuits on fully connected architectures of logarithmic depths are known to be translatable into circuits of depth $\sqrt{n}$ on 2D lattices. Boxio et al. used numerical simulations to optimize strategies to generate random circuits with minimized time to converge to a Porter Thomas distribution, leading to the following algorithm:

1. Initialize in the state $|0\rangle^{\otimes n}$.
2. Apply a Hadamard gate to each qubit.
3. Apply a random circuit with a stack of depth d, where each layer has the following two clock cycles:
   a) Apply a clock cycle of random single-qubit gates to all qubits.
   b) Apply a clock cycle of two-qubits gates.

The gate set consists of the single-qubit gates $\{\sqrt{X}, \sqrt{Y}, T\}$ with

$$\sqrt{X} = \frac{1}{\sqrt{2}} \begin{pmatrix} 1 & -i \\ -i & 1 \end{pmatrix} \tag{3.23}$$

and

$$\sqrt{Y} = \frac{1}{\sqrt{2}} \begin{pmatrix} 1 & -1 \\ 1 & 1 \end{pmatrix} \tag{3.24}$$

being the "square root of X" and the "square root of Y" gates:

$$\sqrt{X}^2 = \left(\frac{1}{\sqrt{2}} \begin{pmatrix} 1 & -i \\ -i & 1 \end{pmatrix} \right)^2 \tag{3.25}$$

$$= \begin{pmatrix} 0 & 1 \\ 1 & 0 \end{pmatrix} \tag{3.26}$$

$$= X \tag{3.27}$$

and

$$\sqrt{Y}^2 = \left(\frac{1}{\sqrt{2}} \begin{pmatrix} 1 & -1 \\ 1 & 1 \end{pmatrix} \right)^2 \tag{3.28}$$

$$= \begin{pmatrix} 0 & -i \\ i & 0 \end{pmatrix} \tag{3.29}$$

$$= Y. \tag{3.30}$$

The circuit can be separated into different layers, where each layer consists of one layer of controlled Z (CZ) gates and one layer of random single-qubit gates. The single-qubit gates are chosen such that each single-qubit gate on qubit q in the current cycle differs from the single-qubit gate on q at the previous cycle.

The 2-qubit CZ gates are applied as demonstrated in figure **??**. Notice that it is not possible to apply a 2-qubit gate to any two qubits in current quantum devices but only to neighboring qubits.

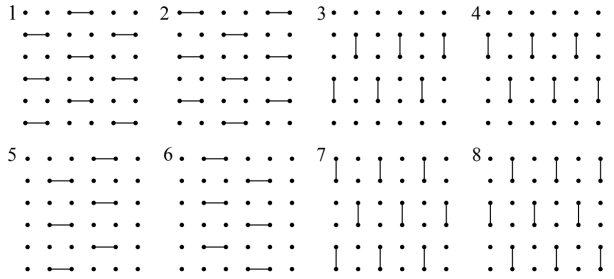

Figure 3.4: Order in which CZ gates are applied to the qubits. As the qubits are aligned on a 2D lattice, only neighboring qubits can be coupled through CZ gates. The pattern repeats every 8 cycles.

Boxio et al. could numerically show that random circuits generated this way generate output distributions according to Porter Thomas after a square root

number of cycles in the number of qubits.

3.5 Experiments on Real Hardware

With an algorithm for the generation of random circuits and a metric for the quality of an execution of such circuits at hand, a team from Google and the UCSB conducted a quantum supremacy experiment on the 54 superconducting qubit *Sycamore* processor, shown in figure **??**.

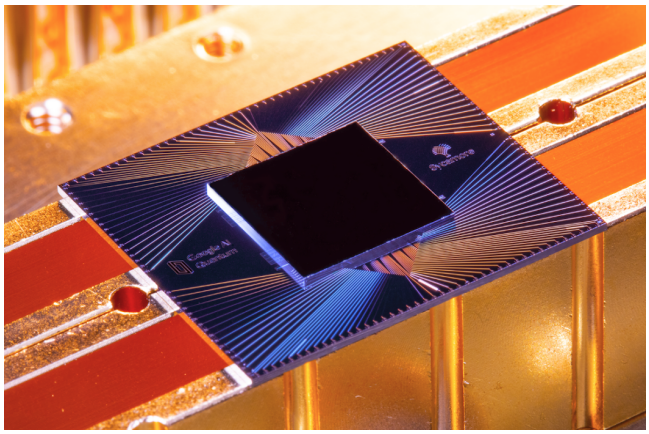

Figure 3.5: The Sycamore processor used in the quantum supremacy experiments of Google and UCSB. It consists of 54 qubits of which one was malfunctioning.

For the experiments, circuits with $n = 10$ to $n = 53$ qubits and $m = 12$ to $m = 20$ cycles have been used. The full cycles generated according to the procedure given above can be classically simulated up to $n = 53$ qubits with $m = 14$ cycles in a reasonable amount of time. Beyond that regime, simplified circuit architectures, called *elided* and *patched*, in which the circuit is split into two sub-circuits with only weak entanglement in the elided and no entanglement in the patched version, allowed the classical simulation for up to $n = 53$ qubits with $m = 20$ cycles to verify the fidelity of the Sycamore processor. For every circuit parameters, 20 circuits have been generated. For each circuit, $0.5 - 2.5$ million samples have been drawn from the quantum processor.

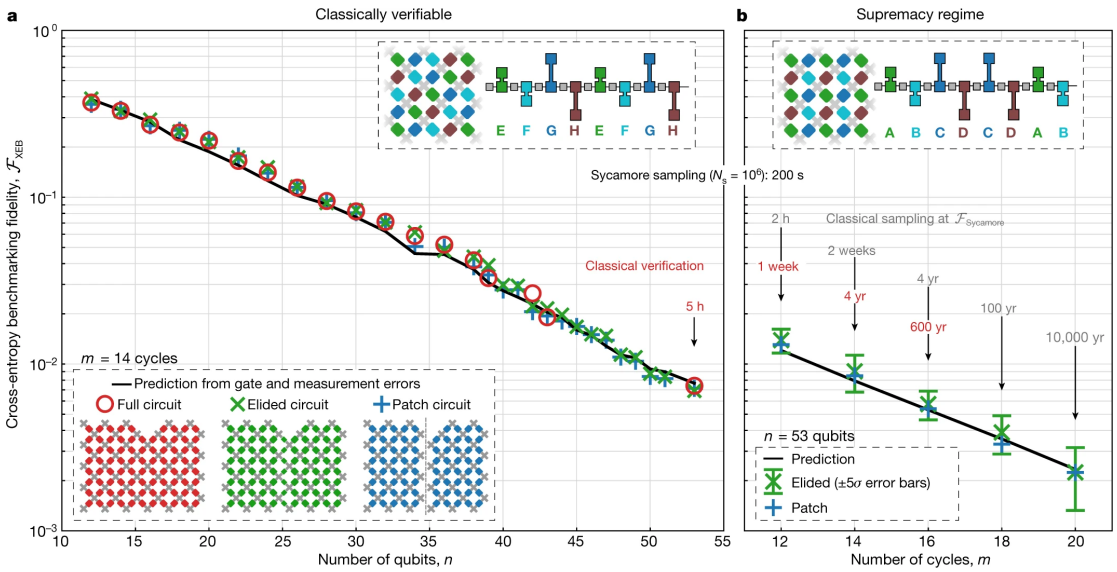

Figure 3.6: Results from the quantum supremacy experiments with the Sycamore processor [**?**]. The full circuits could only be simulated up to $n = 53$ qubits and $m = 12$ cycles. Experiments on elided and patched circuits match the values of the extrapolated cross entropy fidelity.

The team reports an average circuit fidelity $> 0.1\%$ with 5σ confidence for the largest elided circuits. All results fit the extrapolated expected fidelity from smaller circuits, making the team conclude that similar fidelities would be achieved for the full circuits. As classical simulations of these circuits would take up to 100,000 years according to the team with a hybrid Schroedinger-Feynman algorithm, this would imply that quantum supremacy has been achieved. The reported fidelities of the quantum supremacy for the different circuit sizes and depths are reported in figure **??**.

Shortly after these results have been announced, researchers from IBM claimed that the classical simulations for the full circuits on 53 qubits and 20 cycles could have been performed on the Summit supercomputer within a few days only with an optimized memory usage. Experimental proof for these claims is still to be given.

Even if these circuits can be simulated within a few days, the quantum processor would still outperform the classical simulation as it only takes about 200ms to generate the 2 million samples for those circuits from it. As quantum supremacy is a loosely defined term, the discussion might continue whether quantum supremacy has been demonstrated by the Google and UCSB team. Nevertheless, it is an impressive engineering achievement to build a quantum processor of 53 qubits which can execute quantum circuits consisting of up to 1,113 single-qubit and 430 two-qubit gates. For the future, the Google team expects a double exponential growth of the computational power of quantum computers as the classical simulation costs grow exponentially with the computational volume (gates and qubits)

and quantum hardware improvements will probably follow a quantum processor equivalent of Moore's law.

This study does not focus on quantum circuits running on physical quantum devices, but rather on the classical simulation. New and improved classical approximate simulations of quantum systems with neural networks recently proved to work well on many problem instances. Understanding their performance and needed computational resources on the RCS task might provide useful insights about the capabilities and limitations of neural networks for the classical simulation of quantum systems.

4 Boltzmann Machines

The following chapter gives an introduction to Boltzmann machines and their applications to the classical simulation of quantum computing.

An overview of the architecture and mathematical properties of Boltzmann machines are given in the first section. The restricted Boltzmann machine is motivated as a special kind of Boltzmann machine with useful mathematical properties in the second part of this chapter. Afterward, the concepts of Gibbs sampling and supervised learning are explained. In the last section, a constructive approach is given on how restricted Boltzmann machines can be applied to the classical simulation of quantum computing.

The introduction to Boltzmann machines and restricted Boltzmann machines as well as the introduction to Gibbs sampling are based on [**?**] and [**?**] which are also recommended as a more throughout introduction into the topic. The section on supervised learning and gradient descent methods is based on [**?**]. The reader who is already familiar with the concept of Boltzmann machines and how they can be trained in a supervised manner can safely skip to section **??** which is based on the work of Jónsson, Bauer and Carleo [**?**].

4.1 Characteristics

The concept of the Boltzmann machine has first been proposed in the 1980s as a model for parallel distributed computing [**?**]. Boltzmann machines are physically inspired by the Ising Spin model and can be interpreted as energy-based recurrent neural networks representing probability distributions over vectors $\boldsymbol{d}_i \in \{0,1\}^n$ [**?**].

A Boltzmann machine is a network of stochastic units (or neurons) $X = V \cup H$ which are segmented into *visible* neurons $V = \{v_1, \ldots, v_n\}$ and *hidden* neurons $H = \{h_1, \ldots, h_m\}$. The joint state of the visible neurons $\boldsymbol{v} = (v_1 \ldots v_n) \in \{0,1\}^n$ represents n-dimensional data points $\boldsymbol{d}_i \in \{0,1\}^n$ while hidden neurons increase the expressiveness of the Boltzmann machine by acting as non-linear feature detectors to model dependencies between the visible neurons [**?**].

The neurons are connected to each other by weighted links W_{ij} and poss biases a_i (visible) or b_i (hidden) respectively. In the general case, the neurons of a Boltzmann machine can be fully connected. A graphical representation of a fully connected Boltzmann machine is shown in figure **??**.

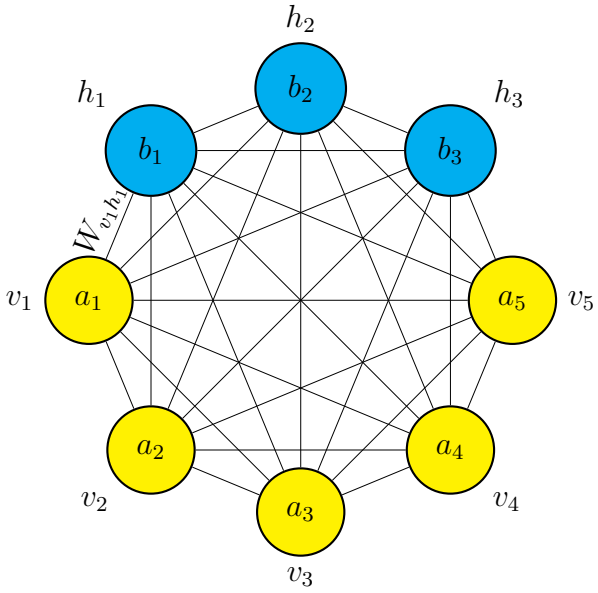

Figure 4.1: Graphical representation of a fully connected Boltzmann machine with 5 visible neurons (yellow) v_1 to v_5 and 3 hidden neurons (blue) h_1 to h_3. Each neuron posses a bias a_1 to a_5 and b_1 to b_3 respectively. The connection weight between two neurons i and j is given by W_{ij}.

Each configuration $\boldsymbol{c} = (v_1, \ldots, v_n, h_1, \ldots, h_m)$ of neuron states of the Boltzmann machine is associated with an energy $E(\boldsymbol{c})$ value which is defined by the parameters $\mathcal{W}$, consisting of its weights and biases $\mathcal{W} = \{a_i, b_i, W_{ij}\}$:

$$E(\boldsymbol{c}; \mathcal{W}) = -\sum_{v_i \in V} a_i v_i - \sum_{h_i \in H} b_i h_i - \sum_{x_i, x_j \in X} W_{x_i, x_j} x_i x_j. \tag{4.1}$$

When sampling configurations from the Boltzmann machine (discussed in more detail in section **??**) the Boltzmann machines prefers low energy states over states with a high energy. The stationary probability of a configuration $\boldsymbol{c}$ with energy $E(\boldsymbol{c}; \mathcal{W})$ is given by the so-called Gibbs-Boltzmann distribution [**?**]:

$$p(\boldsymbol{c}; \mathcal{W}) = \frac{\mathrm{e}^{-E(\boldsymbol{c}; \mathcal{W})}}{Z(\mathcal{W})}, \tag{4.2}$$

where $Z(\mathcal{W})$ is the normalizing partition function

$$Z(\mathcal{W}) = \sum_{\boldsymbol{c\prime} \in C} \mathrm{e}^{-E(\boldsymbol{c\prime}; \mathcal{W})}. \tag{4.3}$$

In a training phase (discussed in section **??**) the parameters of the Boltzmann machine can be adapted in such a way that the marginal probability distribution of the visible neurons

$$p(\boldsymbol{v}; \mathcal{W}) = \sum_{\boldsymbol{h}_k \in \{0,1\}^m} p(\boldsymbol{v}, \boldsymbol{h}_k; \mathcal{W}), \tag{4.4}$$

which traces out the hidden unit states by summing over all possible configurations of them, resembles the probability distribution of data points $\boldsymbol{d}_i$ in a training set $D = \{\boldsymbol{d}_1, \ldots, \boldsymbol{d}_l\}$.

For a fully connected Boltzmann machine, this representation consists of an exponential number of summands and cannot be calculated efficiently. So-called Restricted Boltzmann machines (RBM) have a specific architecture with a restricted connectivity, which allows the efficient calculation of the marginal probability. RBMs and their architectures will be explained in the next section.

4.2 Restricted Boltzmann machines

The so-called Restricted Boltzmann machine (RBM) is an important type of Boltzmann machine with a specific architecture and properties [**?**]. Since their invention, RBMs have been applied to a variety of machine learning tasks and played a key role in the development of deep learning architectures as building blocks of so-called Deep Belief networks [**?**, **?**]. RBMs are also the kind of Boltzmann machines which are being used in this study for the simulation of quantum circuits.

In the restricted case, the neurons of the Boltzmann machine are separated into two layers, one being the visible layer containing the visible neurons $v_i \in V$ and the other layer being the hidden layer containing the hidden neurons $h_j \in H$. Each neuron of the RBM is only allowed to be connected to the neurons from the other layer. Intra-layer connections are not allowed, making the graph of the RBM bipartite, as shown in figure **??**.

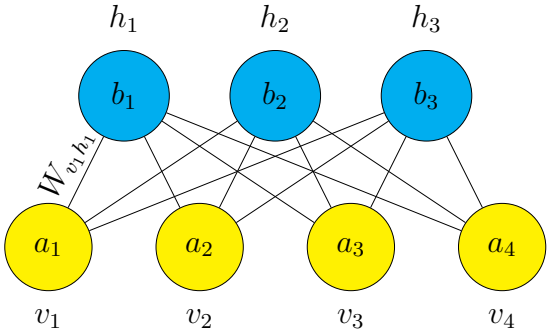

Figure 4.2: Graphical representation of a RBM with 5 visible neurons and 3 hidden ones. There are only connections between the two layers and no connection between two neurons from the same layer.

The marginal probability $p(\boldsymbol{v}; \mathcal{W})$ of the visible neuron states in a RBM has the form

$$p(\boldsymbol{v};\mathcal{W}) = \sum_{\boldsymbol{h}_k\in\{0,1\}^m} p(\boldsymbol{v},\boldsymbol{h}_k;\mathcal{W}) \tag{4.5}$$

$$= \frac{1}{Z(\mathcal{W})} \sum_{\boldsymbol{h}_k\in\{0,1\}^m} \mathrm{e}^{-E(\boldsymbol{v},\boldsymbol{h}_k;\mathcal{W})} \tag{4.6}$$

$$= \frac{1}{Z(\mathcal{W})} \sum_{h_1\in\{0,1\}} \cdots \sum_{h_m\in\{0,1\}} \mathrm{e}^{\sum_{v_i} b_i v_i} \prod_{j=1}^{m} \mathrm{e}^{h_j(b_j+\sum_{i=1}^{n} W_{ij}v_i)} \tag{4.7}$$

$$= \frac{\mathrm{e}^{\sum_{v_i} b_i v_i}}{Z(\mathcal{W})} \sum_{h_1\in\{0,1\}} \mathrm{e}^{h_1(b_1+\sum_{i=1}^{n} W_{i1}v_i)} \cdots \sum_{h_m\in\{0,1\}} \mathrm{e}^{h_m(b_m+\sum_{i=1}^{n} W_{im}v_i)} \tag{4.8}$$

$$= \frac{\mathrm{e}^{\sum_{v_i} b_i v_i}}{Z(\mathcal{W})} \prod_{i=1}^{m} \sum_{h_i\in\{0,1\}} \mathrm{e}^{h_i(b_i+\sum_{i=1}^{n} W_{ij}v_i)} \tag{4.9}$$

$$= \frac{\mathrm{e}^{\sum_{v_i} b_i v_i}}{Z(\mathcal{W})} \prod_{i=1}^{m} (1 + \mathrm{e}^{b_i+\sum_{i=1}^{n} W_{ij}v_i}). \tag{4.10}$$

This quantity consists of only a polynomial number of terms in the number of hidden units of the RBM and can be calculated efficiently. This makes the RBM a compact representation of a probability distribution over vectors $\boldsymbol{d}_i \in D$ inferred from a dataset D.

Even though the RBM has a limited connectivity between its units, it is a universal function approximator [**?**]. It can model any distribution over $\{0,1\}^m$ arbitrary well with m visible and k+1 hidden units, where k denotes the cardinality of the support set of the target distribution, that is, the number of input elements from $\{0,1\}^m$ that have a non-zero probability of being observed. This also implies a worst-case exponential number of hidden units for distributions with an extensive support set [**?**]. It has been shown though that even fewer units can be sufficient depending on the patterns in the support set [**?**].

4.3 Gibbs Sampling

Boltzmann machines are generative models representing probability distributions over their configurations. This means that it is possible to draw configurations from a Boltzmann machine according to their (marginal) probabilities given in equations **??** and **??**.

Though it is required to calculate $Z(\mathcal{W})$ for the exact probabilities of each configuration, it is not necessary to calculate the energies for all the 2^{n+m} possible configurations of a Boltzmann machine to draw samples from it.

Instead, Boltzmann machines can be seen as *Markov chains* with a *stationary probability distribution*. With a stochastic process called *Gibbs sampling*, the samples can be drawn efficiently according to this stationary distribution for RBMs.

This section gives a short introduction into Markov chains, Gibbs sampling and how it can be applied to draw configurations from an RBM.

Gibbs sampling belongs to the class of so-called *Metropolis-Hastings* algorithms and by that is a *Monte Carlo Markov Chain* (MCMC) algorithm [**?**]. It is a simple algorithm to produce samples from the joint probability distribution of multiple random variables like neuron state configurations of a Boltzmann machine, which can be considered as a Markov chain.

A Markov chain is a discrete stochastic process of configurations of random variables $C = \{\boldsymbol{c}^{(t)}\}$ at time steps $t = 1, \ldots, T$ which take values in a set Ω (for Boltzmann machines $\Omega = \{0,1\}^{m+n}$) and for which for all time steps t and for all configurations $\boldsymbol{c}_j, \boldsymbol{c}_i, \boldsymbol{c}_{i-1}, \ldots, \boldsymbol{c}_0 \in \Omega$ the *Markov property*

$$p_{ij}^{(t)} := P(\boldsymbol{c}^{(t+1)} = c_j \mid \boldsymbol{c}^{(t)} = \boldsymbol{c}_i, \ldots, \boldsymbol{c}^{(0)} = c_0) \tag{4.11}$$

$$= P(\boldsymbol{c}^{(t+1)} = c_j \mid \boldsymbol{c}^{(t)} = \boldsymbol{c}_i) \tag{4.12}$$

holds, meaning that the next state of the system only depends on the current state and not on the system's history. A Markov chain can be represented as a (finite) graph as the one shown in figure **??**.

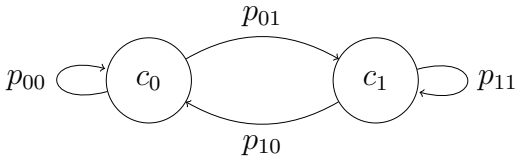

Figure 4.3: A Markov chain with two states c_0 and c_1. The Markov chain is described by the 2×2 matrix $\boldsymbol{P} = \begin{pmatrix} p_{00} & p_{01} \\ p_{10} & p_{11} \end{pmatrix}$.

In the case of Boltzmann machines the transition probabilities p_{ij} are time independent and given by the ratios of configuration probabilities. For RBMs the transition probability p_{ij} from configuration c_i to c_j is given by:

$$p_{ij} = \frac{\mathrm{e}^{\sum_{v_i \in \boldsymbol{c_i}} b_i v_i} \prod_{i=1}^{m} (1 + \mathrm{e}^{b_i + \sum_{i=1}^{n} W_{ij} v_i})}{\mathrm{e}^{\sum_{v_i \in \boldsymbol{c_j}} b_i v_i} \prod_{i=1}^{m} (1 + \mathrm{e}^{b_i + \sum_{i=1}^{n} W_{ij} v_i})}, \tag{4.13}$$

which can be calculated efficiently as the $Z(\mathcal{W})$ terms from equation **??** cancel out.

In each time step t during the Gibbs sampling, the state of a single randomly chosen neuron of the RBM is flipped so that the configurations $\boldsymbol{c}^{(t)}$ and $\boldsymbol{c}^{(t+1)}$ only differ in the state of one neuron. With probability p_{ij} configuration $\boldsymbol{c}_j$ is kept as the new configuration and with probability $1 - p_{ij}$ the Boltzmann machine will stay in its current configuration $\boldsymbol{c}_i$. This corresponds to a random walk on the

Markov chain defined by the RBM transition probabilities. The algorithm is given in algorithm **??**.

Algorithm 1 Gibbs Sampling

Require: $bm(c)$: function returning the energy of a Boltzmann machine for configuration c
Require: T: time steps
1: $t \leftarrow 0$
2: $c^{(0)} \leftarrow randomize(\{0,1\}^{m+n})$ (random initialization)
3: **repeat**
4: $\quad r \leftarrow random(m+n)$
5: $\quad E_i \leftarrow bm(c^{(t)})$
6: $\quad E_j \leftarrow bm(\{c_1, \ldots, \bar{c_r}, \ldots, c_{m+n}\})$
7: $\quad$ **if** $random(1) < \frac{E_i}{E_j}$ **then**
8: $\quad\quad c^{(t+1)} \leftarrow \{c_1, \ldots, \bar{c_r}, \ldots, c_{m+n}\}$
9: $\quad t \leftarrow t+1$
10: **until** $t = T$
11: **return** $c^{(T)}$

The Markov chain for configurations of a Boltzmann machine is known to converge to its so-called *stationary distribution* π, that is

$$\pi^T = \pi^T \boldsymbol{P} \tag{4.14}$$

with $\boldsymbol{P} = (p_{ij})$ being the transition matrix of the Markov chain with the transition probabilities as its entries. Once the Markov chain reaches its stationary distribution, all subsequent states will be distributed according to this distribution.

This means running Gibbs sampling for sufficiently many time steps T will sample configurations according to the Gibbs-Boltzmann distribution given in equation **??**.

Although Gibbs sampling is a straightforward algorithm, it is an important algorithm in the context of Boltzmann machines. Different versions of Gibbs sampling have been developed for RBMs like (persistent) contrastive divergence [**?**, **?**] or parallel tempering [**?**]. In this study, Gibbs sampling will be used in its simplest version, as described in this chapter.

4.4 Supervised Learning

The probability distribution over vector spaces given by a Boltzmann machine can be trained to resemble the distribution of data points $\boldsymbol{d}_i$ in a dataset $D = \{\boldsymbol{d}_1, \ldots, \boldsymbol{d}_d\}$. This can be done either in a *unsupervised* or in a *supervised* manner.

In both cases the parameters $\mathcal{W} = \{\boldsymbol{a}, \boldsymbol{b}, \boldsymbol{W}\}$ of the Boltzmann machine are updated minimizing an objective function $O(\mathcal{W})$ which depends on the parameters of the Boltzmann machine and depicts the overlap of the current and the target distribution in iterative processes like *gradient descent* or *stochastic reconfiguration*.

This section gives a brief introduction into supervised learning and the gradient descent method *Adamax* [**?**] and *stochastic reconfiguration*, another optimization method for RBMs.

Before the training phase, the Boltzmann machine is initialized with random parameters and a training set $D = \{\boldsymbol{d}_1, \ldots, \boldsymbol{d}_d\}$ is given. In the case of supervised learning of Boltzmann machines, the training set consists of tuples of configurations and their corresponding target energy values $\boldsymbol{d}_i = (\boldsymbol{c}_i, t_i)$.

In the batch version of gradient descent, which is being used in this study, the training set D is split into subsets $D_1, \ldots, D_l$, also called *batches*.

For each such batch D_i, the average overlap $O(\boldsymbol{c}_j; \mathcal{W})$ for all $\boldsymbol{c}_j \in D_i$ is computed. Afterwards, the gradients ΔO_x are calculated and the parameters updated into the direction of the steepest descent:

$$\Theta_i = \Theta_i + \Delta O \ldots. \tag{4.15}$$

This process is repeated for a defined number of iterations to minimize the objective function $O(\mathcal{W})$. A graphical representation of this process is shown in figure **??**.

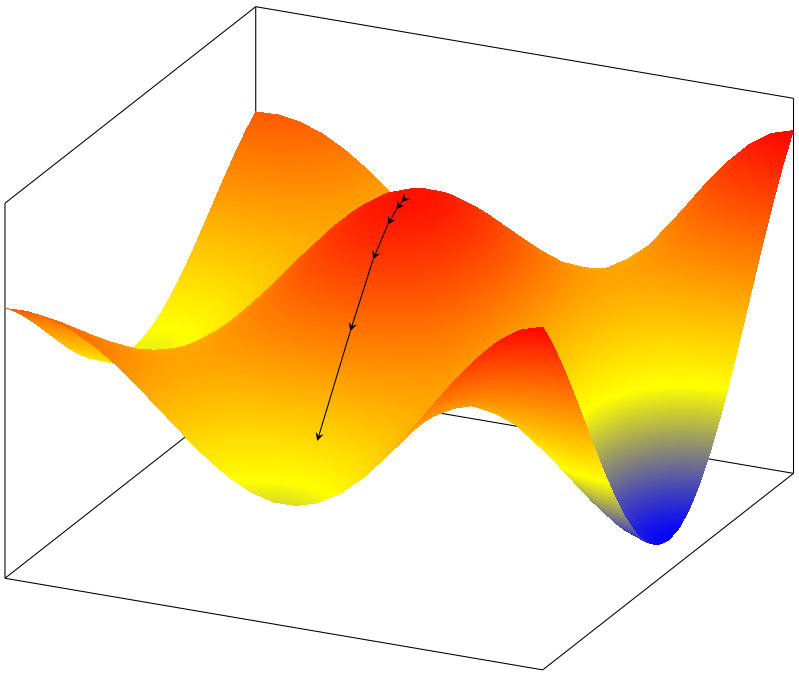

Figure 4.4: Iterations of a gradient descent method. At each iteration, the randomly initialized parameters get updated in direction of the steepest descent of the function to be optimized. After enough iterations, a minimum is of the function is reached.

The simple update rule in **??** has several drawbacks, however. First, The gradient and thus the step size will become smaller as closer the function approaches its minimum, leading to only small improvements and many steps necessary. Second, the function's shape will usually have (many) local minima, which should be avoided. Several variants of gradient descent have been developed to overcome these issues [**?**].

One successful such strategy which is used in this study is called *AdaMax*, a special version of *Adam* [**?**].It combines the advantages of AdaGrad [**?**] and RMSProp [**?**], two other popular gradient descent methods. It is computationally efficient, has little memory requirements, and proves to be well suited for problems with much noise and sparse gradients.

The algorithm updates exponential moving averages of the gradient (mt) and the squared gradient (vt) where the hyper-parameters $\beta_1, \beta_2 \in [0, 1)$ control the exponential decay rates of these moving averages. The moving averages themselves are estimates of the 1st moment (the mean) and the 2nd raw moment of the gradient. The update rule for the parameters Θ_{ij} for Adamax are summarized in algorithm **??**.

Algorithm 2 Adamax

Require: α: step size
Require: $\beta_1, \beta_2 \in [0, 1)$: Exponential decay rates
Require: $f(\Theta)$: Stochastic objective function with parameters $Theta$
Require: Θ_0: Initial parameter vector
$m_0 \leftarrow 0$ (Initialize 1^{st} moment vector)
$u_0 \leftarrow 0$ (Initialize the exponential weighted infinity norm)
$t \leftarrow 0$ (Initialize time step)
while Θ_t not converged **do**
    $t \leftarrow t + 1$
    $g_t \leftarrow \nabla_\Theta f_t(\Theta_{t-1})$ (Get gradients w.r.t. objective function at time step t)
    $m_t \leftarrow \beta_1 \cdot m_{t-1} + (1 - \beta_1) \cdot g_t$ (Update biased first moment estimate)
    $u_t \leftarrow max(\beta_2 \cdot u_{t-1}, |g_t)$ (Update the exponentially weighted infinity norm)
    $\Theta_t \leftarrow \Theta_{t-1} - (\alpha/(1 - \beta_1^t)) \cdot m_t/u_t$ (Update parameters)
return Θ_t (Resulting parameters)

4.5 Application to Quantum Computing

Machine learning techniques have become a successful approach for the classical simulation of quantum systems [**?**, **?**, **?**]. Carleo and Troyer [**?**] have first given a compact presentation of the wavefunction of a many-body quantum system with an RBM. The same framework has later been used by Jónsson, Bauer, and Carleo for the classical simulation of the quantum Fourier and Hadamard transform [**?**]. Their work gives a constructive approach on how the parameters of a complex-valued RBM representing the quantum state

$$\Psi_{\mathcal{W}}(\boldsymbol{v}) = \frac{\mathrm{e}^{\sum_{v_i} b_i v_i}}{Z(\mathcal{W})} \prod_{i=1}^{m} (1 + \mathrm{e}^{b_i + \sum_{i=1}^{n} W_{ij} v_i}) \tag{4.16}$$

can be adapted to apply a universal set of quantum gates to the quantum state $\Psi_{\mathcal{W}}$.

RBMs allow only an exact application of unitary gates diagonal in the computational basis. For non-diagonal gates more hidden layers would be necessary, making the calculation of the quantum state intractable [**?**]. Nevertheless, it is possible to train a Boltzmann machine in a supervised fashion, so its parameters are adapted to apply a non-diagonal gate to its state approximately.

The rules for the applications of diagonal and non-diagonal gates to an RBM state from [**?**] detailed in following two sections.

4.5.1 Diagonal gates

Diagonal gates can be applied to an RBM quantum state by solving a set of linear equations. This section describes the rules for the applications of single-qubit Z

rotations, controlled Z rotations as well as the Pauli X, Y and Z gates.

Single-Qubit Z rotations

The action of the single Z rotation of angle θ is given by the 2×2 unitary matrix

$$\begin{pmatrix} 1 & 0 \\ 0 & \mathrm{e}^{i\theta} \end{pmatrix}. \tag{4.17}$$

Its action on qubit l yields $\langle \boldsymbol{v} \mid R_l^z(\theta) \mid \Psi_W \rangle = \mathrm{e}^{i\theta v_l} \Psi_W(\boldsymbol{v})$. Considering a RBM machine with weights $\mathcal{W}' = \{\alpha', \beta', W'\}$, the action of the $R^Z(\theta)$ gate is exactly reproduced if $\mathrm{e}^{v_l a_l} \mathrm{e}^{i\theta v_l} = \mathrm{e}^{v_l a'_l}$ is satisfied, which is the case for

$$a'_j = a_j + \delta_{jl} i\theta. \tag{4.18}$$

The action of the Z rotation thus simply modifies the bias of the visible neuron l of the RBM.

Controlled Z rotations

The action of a controlled Z rotations acting on two given qubits l and m is determined by the 4×4 unitary matrix:

$$\begin{pmatrix} 1 & 0 & 0 & 0 \\ 0 & 1 & 0 & 0 \\ 0 & 0 & 1 & 0 \\ 0 & 0 & 0 & \mathrm{e}^{i\theta} \end{pmatrix} \tag{4.19}$$

where θ is a given rotation angle. This gate is diagonal and can compactly be written as

$$\langle \boldsymbol{v} \mid CZ(\theta) \mid \Psi_W \rangle = \mathrm{e}^{i\theta v_l v_m} \Psi_W(v_1 \dots v_n). \tag{4.20}$$

As the RBM architecture does not allow direct interaction between visible neurons, the CZ gate requires the insertion of a dedicated extra hidden unit h_c, which is connected to the qubits l and m:

$$\langle \boldsymbol{v} \mid CZ(\theta) \mid \Psi_W \rangle = \mathrm{e}^{\Delta a_l B_l + \Delta a_m Z_m} \sum_{h_c} \mathrm{e}^{W_{lc} B_l h_c + W_{mc} B_m h_c} \tag{4.21}$$

$$= \mathrm{e}^{\Delta a_l B_l + \Delta a_m B_m} \times (1 + \mathrm{e}^{W_{lc} B_l + W_{mc}} B_m) \Psi_W(\mathcal{B}), \tag{4.22}$$

where the new weights W_{lc} and W_{mc} and visible units biases $a_l\prime = a_l + \Delta a_l$, $a_m\prime = a_m + \Delta a_m$ are determined by the equation:

$$\mathrm{e}^{\Delta a_l B_l + \Delta a_m B_m} (1 + \mathrm{e}^{W_{lc} B_l + W_{mc} B_m}) = C \times \mathrm{e}^{i\theta B_l B_m} \tag{4.23}$$

for all the four possible values of the qubits values $B_l, B_m = \{0, 1\}$ and where C is an arbitrary (finite) normalization. A possible solution for this system is:

$$W_{lc} = -2\mathrm{A}(\theta) \tag{4.24}$$

$$W_{mc} = 2\mathrm{A}(\theta) \tag{4.25}$$

$$\Delta a_l = i\frac{\theta}{2} + \mathrm{A}(\theta) \tag{4.26}$$

$$\Delta a_m = i\frac{\theta}{2} - \mathrm{A}(\theta) \tag{4.27}$$

where $\mathrm{A}(\theta) = arccosh(\mathrm{e}^{-i\frac{\theta}{2}})$. Modifying the RBM's parameters accordingly will apply a CZ gate to its current state.

Pauli X gate

The X gate just flips the qubit l and the RBM amplitudes are:
$\langle \boldsymbol{v} \mid X_l \mid \Psi_W \rangle = \langle v_1 \dots \bar{v_l} \dots v_N \mid \Psi_W \rangle$.
Since $\bar{v_l} = (1 - v_l)$, it must be satisfied that

$$(1 - v_l)W_{lk} + b_k = v_l W_{lk}\prime + b_k\prime \tag{4.28}$$

and

$$(1 - B_l)a_l = B_l a_l\prime + C \tag{4.29}$$

hold for all the (two) possible values of $B_l = \{0, 1\}$. The solution is simply:

$$W_{lk}\prime = -W_{lk} \tag{4.30}$$

$$b_k\prime = b_k + W_{lk} \tag{4.31}$$

$$a_l\prime = -a_l \tag{4.32}$$

$$C = a_l \tag{4.33}$$

whereas all the a_j and the other weights W_{jk} with $j \neq i$ are unchanged.

Pauli Y gate

A similar solution is also found for the Y gate, with the noticeable addition of extra phases with respect to the X gate:

$$W_{lk}\prime = -W_{lk} \tag{4.34}$$

$$b_k\prime = b_k + W_{lk} \tag{4.35}$$

$$a_l\prime = -a_l + i\pi \tag{4.36}$$

$$C = a_l + \frac{i\pi}{2} \tag{4.37}$$

whereas all the a_j and other weights W_{jk} with $j \neq l$ are unchanged.

Pauli Z gate

The Pauli Z gate is a special case of the Z rotation with $\theta = \pi$. Thus the only change necessary is to set the bias a_l of the visible neuron l to

$$a_l\prime = a_l + i\pi. \tag{4.38}$$

4.5.2 Non-diagonal gates

Exact applications of non-diagonal gates to Boltzmann machine quantum states would require introducing a second hidden layer [**?**]. In contrast to an RBM with just one hidden layer, this would make the calculation of the represented quantum state inefficient.

Thus, there are no rules for applying non-diagonal gates to an RBM state similar to those for diagonal gates. Nevertheless, the parameters of the RBM can be adapted in a supervised learning process instead.

The training set consists of samples drawn from the RBM with its current set of parameters. In the sampling process, the RBM's energy function can be adapted to resemble the energy states after a non-diagonal unitary gate G has been applied to its state.

For any non-diagonal unitary gate

$$G = \begin{pmatrix} a & b \\ c & d \end{pmatrix} \tag{4.39}$$

applied to qubit l, samples from the state $|\Phi(\boldsymbol{v})\rangle = G_l\,|\Psi(\boldsymbol{v})\rangle$ can be drawn according to

$$|\,|\Phi(\mathcal{B}_{\mathcal{B}_l=0})\rangle\,|^2 = |a \cdot |\Psi(\mathcal{B}_{\mathcal{B}_l=0})\rangle + c \cdot |\Psi(\mathcal{B}_{\mathcal{B}_l=1})\rangle|^2 \tag{4.40}$$

when the state of qubit l is sampled to be 0 and

$$||\Phi(\mathcal{B}_{\mathcal{B}_l=1})\rangle|^2 = |b \cdot |\Psi(\mathcal{B}_{\mathcal{B}_l=0})\rangle + d \cdot |\Psi(\mathcal{B}_{\mathcal{B}_l=1})\rangle|^2 \tag{4.41}$$

when the state is sampled to be 1. The sampling happens according to the squared norm $|\Phi|^2$ to draw the samples according to the probability distribution of the corresponding quantum state.

The samples are then being used to minimize the log-likelihood $L(\mathcal{W})$ of the overlap of the two quantum states Ψ and Φ

$$L(\mathcal{W}) = -\log O(\mathcal{W}) \tag{4.42}$$

$$= -\log \sqrt{\frac{|\langle \Psi_{\mathcal{W}} \mid \Phi \rangle|^2}{\langle \Psi_{\mathcal{W}} \mid \Psi_{\mathcal{W}} \rangle \langle \Phi \mid \Phi \rangle}} \tag{4.43}$$

$$= -\log \sqrt{\left\langle \frac{\Phi(\mathcal{B})}{\Psi_{\mathcal{W}}(\mathcal{B})} \right\rangle_{\Psi} \left\langle \frac{\Psi_{\mathcal{W}}(\mathcal{B})}{\Phi(\mathcal{B})} \right\rangle_{\Phi}^{*}} \tag{4.44}$$

with

$$\langle F(\mathcal{B}) \rangle_A := \frac{\sum_{\mathcal{B}} F(\mathcal{B}) |A(\mathcal{B})|^2}{\sum_{\mathcal{B}} |A(\mathcal{B})|^2} \tag{4.45}$$

by some optimization method. The gradients of this function with respect to the parameters of the Boltzmann machine have the form

$$\partial_{p_k} L(\mathcal{W}) = \langle \mathcal{O}_k^*(\mathcal{B}) \rangle_{\Psi} - \frac{\langle \frac{\Phi(\mathcal{B})}{\Psi(\mathcal{B})} \mathcal{O}_k^*(\mathcal{B}) \rangle_{\Psi}}{\langle \frac{\Phi(\mathcal{B})}{\Psi(\mathcal{B})} \rangle_{\Psi}} \tag{4.46}$$

with $\mathcal{O}_k(\mathcal{B}) = \partial_{p_k} \log \Psi_{\mathcal{W}}(\mathcal{B})$ being the variational derivatives of the RBMs wavefunction with respect to its parameters. These are simple to compute as well, since

$$\partial_{a_i} \log \Psi_{\mathcal{W}}(\boldsymbol{v}) = v_i \tag{4.47}$$

$$\partial_{b_i} \log \Psi_{\mathcal{W}}(\boldsymbol{v}) = h_i \tag{4.48}$$

$$\partial_{W_{ij}} \log \Psi_{\mathcal{W}}(\boldsymbol{v}) = v_i h_j. \tag{4.49}$$

After the training, which happens for a predefined number of iterations on batches of the training set, the quantum state $\Psi_{\mathcal{W}}$ represented by the RBM approximates the target state Φ. Using this approach and AdaMax as the optimization method, Jónsson et al. reported a per gate error of 10^{-3} [**?**].